# Postprint

This document is the Accepted Manuscript version of a Published Work that appeared in final form in  *JACS*

after peer review and technical editing by the publisher.


To access the final edited and published work see:

Thorsten G. Lohr, José I. Urgel, Kristjan Eimre, Junzhi Liu, Marco Di Giovannantonio, Shantanu Mishra, Reinhard Berger, Pascal Ruffieux, Carlo A. Pignedoli, Roman Fasel, and Xinliang Feng

On-Surface Synthesis of Non-Benzenoid Nanographenes by Oxidative Ring-Closure and Ring-Rearrangement Reactions

# On-Surface Synthesis of Non-benzenoid Nanographenes by Oxidative Ring-Closure and Ring-Rearrangement Reactions

Thorsten G. Lohr,[†,¶] José I. Urgel,[‡, φ,¶,*] Kristjan Eimre,[‡,¶] Junzhi Liu,[#,*] Marco Di Giovannantonio,[‡] Shantanu Mishra,[‡] Reinhard Berger,[†] Pascal Ruffieux,[‡] Carlo A. Pignedoli,[‡] Roman Fasel,[‡,Δ,*] and Xinliang Feng[†,*]

[†]Center for Advancing Electronics and Faculty of Chemistry and Food Chemistry, Technical University of Dresden, 01062 Dresden, Germany

[‡]Empa, Swiss Federal Laboratories for Materials Science and Technology, Überlandstrasse 129, 8600 Dübendorf, Switzerland

[φ]IMDEA Nanoscience, C/ Faraday 9, Campus de Cantoblanco, 28049 Madrid, Spain

[#]Department of Chemistry and State Key Laboratory of Synthetic Chemistry, The University of Hong Kong, Pokfulam Road, Hong Kong, China

[Δ]Department of Chemistry and Biochemistry, University of Bern, Freiestrasse 3, 3012 Bern, Switzerland

**ABSTRACT:** Nanographenes (NGs) have gained increasing attention due to their immense potential as tailor-made organic materials for nanoelectronics and spintronics. They exhibit a rich spectrum of physicochemical properties that can be tuned by controlling the size, the edge structure or by introducing structural defects in the honeycomb lattice. Here, we report the design and on-surface synthesis of NGs containing several odd-membered polycycles induced by a thermal procedure on Au(111). Our scanning tunneling microscopy, non-contact atomic force microscopy and scanning tunneling spectroscopy measurements, complemented by computational investigations, describe the formation of two non-benzenoid NGs (**2A** and **2B**) containing four embedded azulene units in the polycyclic framework, via on-surface oxidative ring-closure reactions. Interestingly, we observe surface-catalyzed skeletal ring rearrangement reactions in the NGs, which lead to the formation of additional heptagonal rings as well as pentalene and *as*-indacene units in **2A** and **2B**, respectively. Both **2A** and **2B** on Au(111) exhibit narrow experimental frontier electronic gaps of 0.96 and 0.85 eV, respectively, and Fermi level pinning of their HOMO together with considerable electron transfer to the substrate. Ab initio calculations estimate moderate open-shell biradical characters for the NGs in gas phase.

## INTRODUCTION

Graphene-based materials have attracted tremendous interest in the science and technology field since the successful isolation of graphene in 2004.[1] In the last decades, numerous experimental studies have confirmed that graphene exhibits unique mechanical,[2] magnetic,[3] optical[4] and electronic[5] properties with prospects in future devices.[6–11] For instance, charge carriers in graphene behave like massless Dirac fermions, which results in many new physics phenomena.[12] Despite its unique properties, graphene also presents several drawbacks. For instance, it possesses a zero band gap, which hinders its application as an electronic switch. Remarkably, tailoring the electronic and optical properties of graphene is possible by controlling the size,[13] the edge structure[14] or by introducing structural defects like pentagons, heptagons, or octagons and combinations thereof in the honeycomb lattice.[15,16]

Therefore, the synthesis of well-defined nano-sized graphene fragments (nanographenes, NGs), also known as extended polycyclic aromatic hydrocarbons (PAHs), has recently captivated the interest of the scientific community.[17–19] NGs present electronic gaps of a few eV due to quantum confinement, they are suggested to have toxicity much lower[20] than that of inorganic quantum dots and can be used as model π-electron systems in chemistry. In addition, PAHs containing unpaired electrons (open-shell PAHs) have received increased interest in recent years due to potential applications in organic spintronics.[21] To date, most reported NGs consist exclusively of benzenoid rings. Nevertheless, the controlled introduction of structural defects, i.e. odd-membered polycycles (pentagons or heptagons), in the honeycomb lattice may have a considerable impact on the physicochemical properties of NGs, arising from local changes in strain and conjugation.[22–25]

Under this scenario, atomically-precise bottom-up approaches have provided in the last decades an appealing playground for the design and investigation of NGs with perfectly defined structures and properties,[24,26–36] in contrast to the well-known disadvantages such as non-regular edge structures or uncontrollable sizes presented by the top-down approach.[37] In this regard, on-surface chemical reactions have proven to be a versatile tool for the formation of stable molecular graphene structures that cannot be synthesized in solution.
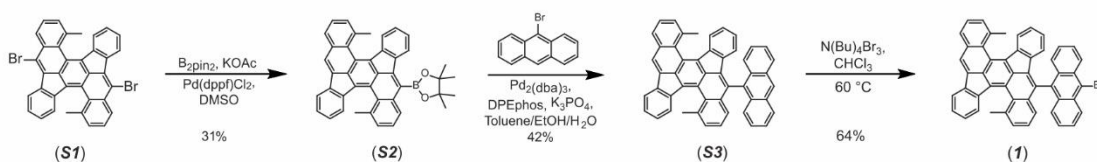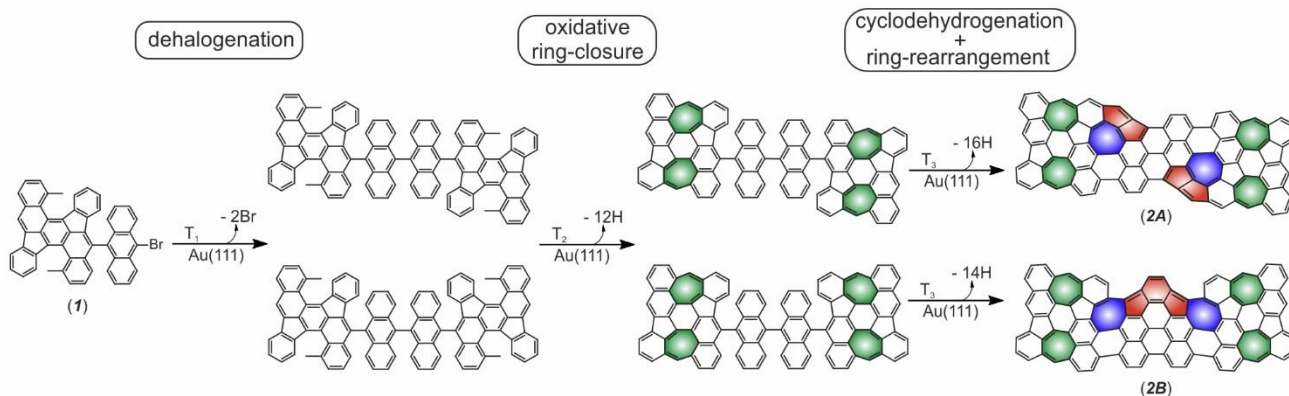
**Scheme 1.** Synthesis of non-benzenoid NGs **2A** and **2B** reported in this work. Colored rings highlight the formation of heptagons via oxidative ring-closure (depicted in green) and cyclodehydrogenation (depicted in blue), and pentalene (**2A**) and *as*-indacene (**2B**) moieties via ring-rearrangement (depicted in red).

Over the last decades, reactions such as Ullmann coupling, imine coupling, alkyne homocoupling or cyclodehydrogenation among others, have been studied with ultimate spatial resolution on single-crystal metal surfaces.[38,39] However, on-surface investigations of other fundamental chemical reactions with important implications in organic synthesis have remained scarce. For instance, rearrangement reactions[40] have been shown to be important in areas of chemical research and industry, representing an excellent alternative to induce the formation of novel nanostructures that are not accessible otherwise. Only recently, a few rearrangement reactions[41–44] including Fritsch–Buttenberg–Wiechell (FBW)[45] and Bergman Cyclization[46,47] have been studied on surfaces. Therefore, further investigations regarding this type of chemical reactions are imperative in order to access molecular mechanistic insights.

In this article, we report the on-surface synthesis of NGs containing odd-membered polycycles, predicted to be open-shell in gas phase by DFT calculations, on a coinage metal surface under ultra-high vacuum (UHV) conditions (Scheme 1). To this end, we synthesized precursor (**1**), which contains 1,10-dimethyldibenzo[*a,m*]rubicene as core motif with additional anthracene moieties that can be sublimed intactly and converted to the NGs (**2A** and **2B**) by thermal activation on the metal surface. Our molecular-level investigations reveal the formation of embedded azulene units in the polycyclic framework of the NGs via on-surface oxidative ring-closure reactions of the methyl substituents, as recently reported in previous studies.[24] Notably, the core of the NGs contains a unique combination of pentagonal and hexagonal rings, *i.e.* pentalene and *as*-indacene formed via surface-catalyzed ring-rearrangement reactions. Such observations highlight the capability to exploit on-surface synthesis protocols in the investigation of ring rearrangement reactions. The chemical structure of the targeted nonbezenoid NGs has been determined by scanning tunneling microscopy (STM) and non-contact atomic force microscopy (nc-AFM), and complemented by density-functional theory (DFT) calculations. In addition to our detailed chemical and structural investigation, we have performed scanning tunneling spectroscopy (STS) measurements to characterize their electronic structure. We observe considerable

charge transfer from the NGs to the substrate. Theoretical characterization shows moderate open-shell character for the final compounds and provides insight into the mechanisms propelling the ring-rearrangement reaction.

## RESULTS AND DISCUSSION

Precursor **1** was synthesized in three steps from 5,14-dibromo-1,10-dimethyldibenzo[*a,m*]rubicene (**S1**) (Scheme 1).[24] Compound **S1** was first borylated to the corresponding boronic ester. The reaction led to a mixture of mono-borylated compound **S2** (yield 31%) and bis-borylated compound **S2B** (yield 42%), which were separated by column chromatography. The Suzuki coupling of compound **S2** with 9-bromoanthracene gave compound **S3** with a yield of 42%, followed by bromination toward precursor **1** (see Supporting Information for detailed procedures and characterization).

After sublimation of **1** onto an atomically clean Au(111) surface held at room temperature and subsequent annealing to 340°C ($T_3$ in Scheme 1), large-scale STM images (Figure 1a) reveal the predominant presence of rectangle-shaped NGs. Some of these NGs are fused together, which is attributed to non-selective CH bond activation that occurs at the same temperature as the formation of the expected NGs. High-resolution STM images shown in Figure 1b-d allow us to clearly discern two different NGs, namely a linear species (blue dashed rectangle) and a curved variant **2B** (green dashed rectangle) that we attribute to **2A** and **2B**, respectively. Such NGs are compatible with the formation of dimers *via* dehalogenative aryl-aryl coupling of **1** and subsequent cyclodehydrogenation and oxidative cyclization reactions (see Figure S1 for RT phase of **1** and intermediate temperature STM images, which correspond to $T_1$ and $T_2$ in Scheme 1, toward the formation of **2A** and **2B**). The presence of two types of dimers arises from the two possible ways that **1** can adsorb on the surface.

To access the chemical structures of **2A** and **2B**, we performed nc-AFM measurements using a carbon monoxide (CO)-functionalized tip.[48] Figure 1e,f depict the constant-height frequency-shift nc-

AFM images. Both **2A** and **2B** adopt a planar conformation on the surface, which is in accordance with the DFT-optimized structures
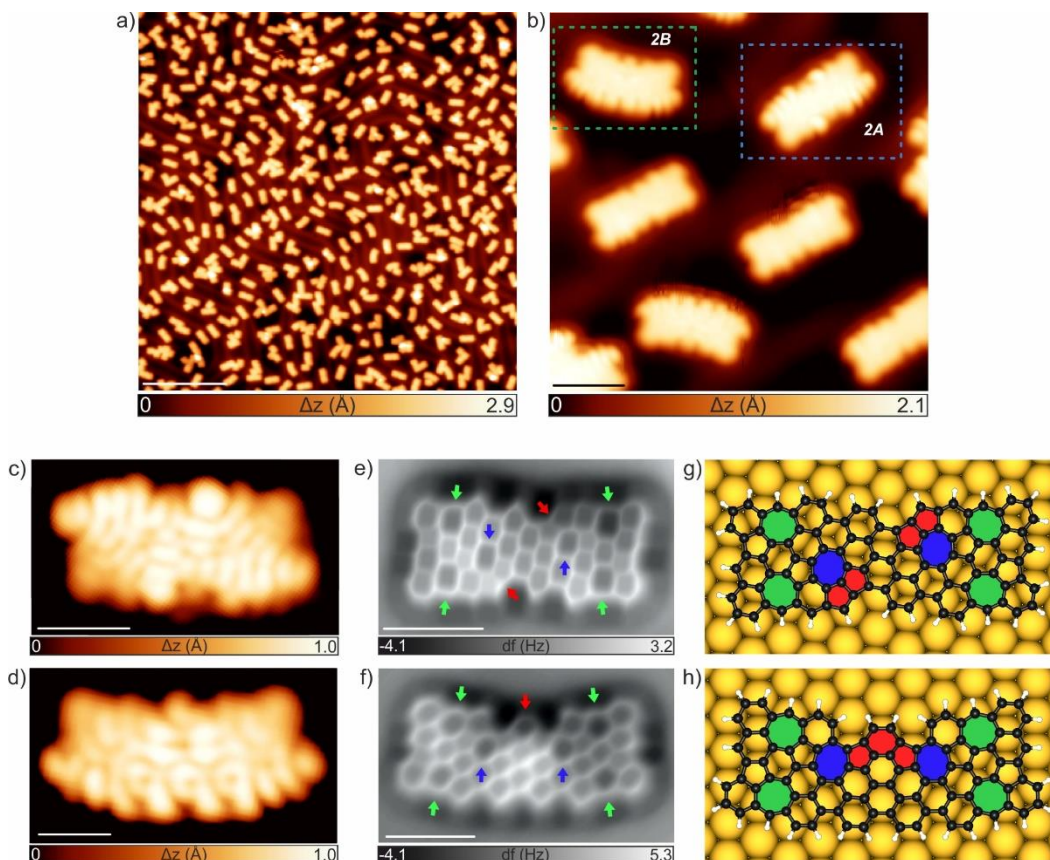


**Figure 1. On-surface synthesis of non-benzenoid NGs 2A and 2B on Au(111).** a) Overview STM topography image of the surface after annealing at 340°C, revealing the predominant presence of **2A** and **2B** . $V_b = -1.0$ V, $I_t = 100$ pA, scale bar: 20 nm. b) Zoom-in high-resolution STM image of (a) acquired with a CO-functionalized tip. $V_b = 0.1$ V, $I_t = 200$ pA, scale bar: 1 nm. c,d) High-resolution STM images, acquired with a CO-functionalized tip, of isolated **2A** and **2B** NGs, respectively. c) $V_b = 0.02$ V, $I_t = 70$ pA. d) $V_b = 0.02$ V, $I_t = 100$ pA. Scale bars: 1 nm. e,f) Constant-height frequency-shift nc-AFM images of panels (c) and (d) acquired with a CO-functionalized tip (z offset −30 pm below STM set point: 5 mV, 70 pA). Scale bars = 1 nm. g,h) Top views of the DFT equilibrium geometries of **2A** and **2B**. Heptagons highlighted in green and blue are formed via oxidative ring-closure of the methyl substituents and cyclode-hydrogenation, respectively, while the pentalene (g) and *as*-indacene (h) moieties highlighted in red are formed via surface-catalyzed ring-rearrangement reactions.

of **2A** and **2B** on Au(111) revealing a planar adsorption with an adsorption height of 3.3 Å with respect to the underlying surface (Figure 1g,h). Furthermore, oxidative ring closure of the four methyl substituents affords the formation of four heptagonal rings toward the termini of both NGs (green arrows and green-filled heptagons in Figure 1e,f and Figure 1g,h respectively).[24,28] Interestingly, the cyclodehydrogenation reactions expected to occur at the center of **2A** and **2B** gave rise to an unforeseen ring rearrangement in the molecular backbone. Herein, two hexagons from the former anthracene segments were rearranged into two pentalene units for **2A** (red arrows and red-filled pentagons in Figure 1e,g respectively) and an *as*-indacene unit for **2B** (red arrows and red-filled hexagon and pentagons in Figure 1f,h respectively), with the concomitant formation of another two heptagonal rings for both **2A** and **2B** (blue arrows and blue-filled heptagons in Figure 1e,f and Figure 1g,h respectively). Such ring-rearrangement reactions as well as the pentalene and *as*-indacene segments formed are rarely observed in the synthesis of organic compounds on surfaces and therefore investigations on these reactions have remained scarce.[43] We note that the NGs that should be formed from cyclodehydro-genation and oxidative cyclization reactions of **1** without undergo-ing any ring-rearrangement reactions (that is, **2A-e** and **2B-e**) would exhibit highly strained structural conformations on Au(111), with strain energies around 0.75 eV as found by our DFT calcula-tions (Figure S2). This considerable strain is likely the driving force

behind the ring rearrangement reactions, which are further facili-tated by the underlying surface (see Figure S3 for the proposed re-action mechanism).

A statistical distribution of the reaction products indicates that after annealing at 340°C, 77% of the NGs formed on the surface present the expected rectangular shape (with equal populations of **2A** and **2B)**, while the remaining 23% of the species corresponds to fused oligomers (with 5% attributed to two fused **2A**/**2B** NGs, 8% to a **2A**/**2B** NG fused to a molecular precursor with one radical position passivated by hydrogen from the residual hydrogen partial pres-sure, and the remaining 10% to ill-defined oligomers). High-reso-lution STM imaging at low bias voltages with a CO-functionalized tip reveals that all curved NGs (as-signed to **2B**) exhibit the same appearance, but the linear NGs (previously assigned to the fully conjugated species **2A**) present two slightly different appearances (Figure 2). From constant-current STM imaging alone (statistics out of ~ 500 NGs), a majority of the linear NGs (65%) exhibit a characteristic two-lobed local density of states (LDOS) feature typ-ical of **2A** (highlighted with arrows in Figure 2c). However, the remaining 35% exhibit no such LDOS feature (Figure 2a), we refer to these NGs as **2A'**. Further differences are resolved in the corre-sponding bond-resolved ultrahigh-resolution STM (UHR-STM) images (Figure 2b,d).[49,50] The UHR-STM image of **2A** (Figure 2d) reveals strong convolution of LDOS with structural features, which

obscures the bond resolution. Since UHR-STM images are acquired at low tunneling biases (typically, $|V| \leq 5$ mV), this observation indicates the presence of considerable LDOS in the NG near the Fermi energy. Conversely, UHR-STM imaging of **2A´** (Figure 2b) does not present any LDOS near the Fermi energy, and leads to clear resolution of the structural features. However, a notable difference exists in the appearance of the outer pentagonal rings of the two pentalene units: while the pentagonal ring at the lower part of the NG (highlighted by a green arrow) reveals a smooth apex, the one at the upper part of the NG (highlighted by a red arrow) reveals a sharp kink at the apex, which has previously been observed for –CH₂ groups.[24,51] We thus propose that the apical carbon atom of the upper pentagonal ring is saturated with two H atoms, which is further confirmed by nc-AFM images of **2A´** which reveal a feature of increased frequency shift localized at the apex of one pentagon (see Figure S4). With the identities of **2A** and **2B** determined, we next investigated the possibility of generating the fully conjugated NG **2A** from **2A´** *via* STM tip-induced hydrogen removal (Figure 2f).To do so, we located the tip at the center of **2A´** and turned the feedback loop off at the setpoint conditions $V_b = 100$ mV and $I_t = 5$ pA. Upon increasing the tunneling voltage $V_b$ to ~ 3.6 V for a few seconds, we reproducibly observed an abrupt change in the tunneling current, which is attributed to a successful manipulation event.[24,44,52,53] UHR-STM images taken after such tip-induced H-cleavage indeed reveal the successful transformation of **2A´** into **2A**.
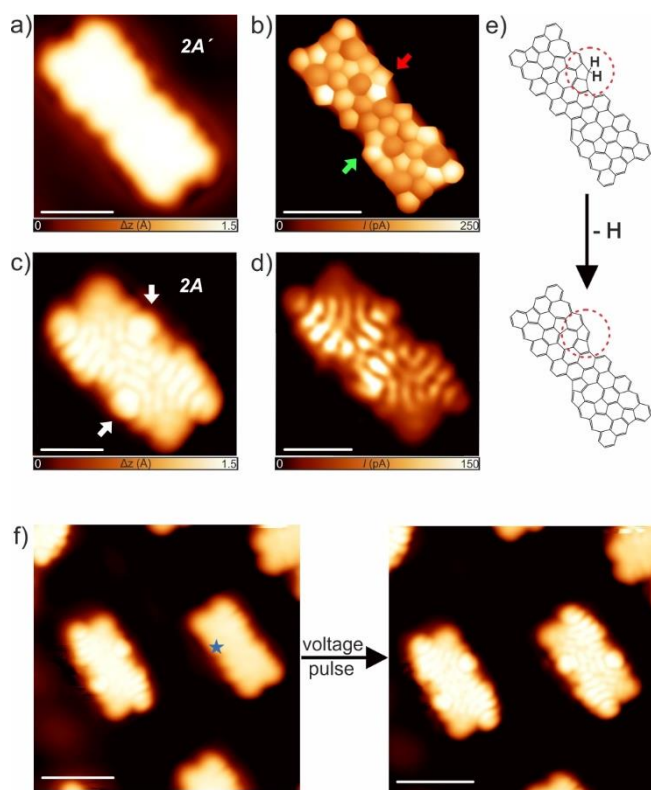


**Figure 2. Transformation of 2A´ into 2A via STM tip-induced H-cleavage.** (a,b) High-resolution STM image of an individual **2A´** nanographene and its corresponding UHR-STM image acquired with a CO-functionalized

tip. The non-benzenoid framework appears completely undistorted as observed in (b). (c,d) High-resolution STM image of an individual **2A** nanographene and its corresponding UHR-STM image acquired with a CO-functionalized tip. In this case, the chemical structure of the nanographene **2A** appears strongly convoluted with the LDOS as observed in (d). e) Chemical sketch illustrating the controlled removal of a hydrogen atom from **2A´** which contains a doubly hydrogenated pentagonal apex to form **2A**. f) High-resolution STM images that show the generation of **2A** through voltage-pulse-induced dissociation of individual hydrogen atoms from **2A´**. The blue star indicates the position of the tip where the voltage pulse was realized. Scanning parameters: a) $V_b = 50$ mV, $I_t = 80$ pA. b) open feedback parameters: $V_b = 5$ mV, $I_t = 50$ pA; $\Delta z = -0.5$ Å. c) $V_b = 17$ mV, $I_t = 150$ pA. d) open feedback parameters: $V_b = 5$ mV, $I_t = 50$ pA; $\Delta z = -0.5$ Å. f) Left: $V_b = 50$ mV, $I_t = 80$ pA, Right: $V_b = 20$ mV, $I_t = 100$ pA. Scale bars: 1 nm.

Next, we performed STS measurements on **2A** and **2B** to probe their electronic structure. For **2A** (Figure 3a), differential conductance (d$I$/d$V$) spectra show prominent peaks in the density of states at +17 mV and +980 mV. These peaks can be assigned respectively to the HOMO and hybridized LUMO/LUMO+1 of **2A** by comparison to a DFT-based projected density of states analysis of the **2A**/Au(111) system (Figure 3a,b; HOMO and LUMO refer to the highest occupied and the lowest unoccupied molecular orbitals, respectively). The projection analysis was performed on closed-shell gas phase orbitals as the molecules did not exhibit spin polarization on the Au(111) substrate. For **2B** (Figure 3d,e), the results are qualitatively similar: the HOMO is found at -20 mV and the hybridized LUMO/LUMO+1 at +830 mV. Therefore, the measured HOMO-LUMO gaps of these non-benzenoid nanographene are found to be ~0.96 and ~0.85 eV on Au(111), respectively, for **2A** and **2B**. Constant-height mapping of the d$I$/d$V$ signal at the energetic positions of the HOMO and the LUMO/LUMO+1 resonances, together with the corresponding STM topography images of **2A** (Figure 3c) and **2B** (Figure 3f) allow us to visualize the spatial distribution of these states. The DFT-calculated local density of states (LDOS) maps at the corresponding resonances, evaluated at a height of 3 Å above the molecular plane, exhibit an excellent agreement with the experimental d$I$/d$V$ maps, which confirms the assignment of the states to molecular orbital resonances (see Figure S5 for experimental and calculated d$I$/d$V$ maps assigned also to HOMO-1 and HOMO-2 for **2A** and **2B**). The experimental d$I$/d$V$ maps and computational PDOS results show that the HOMO resonance is located very close to the Fermi level and is partially unoccupied, i.e. the HOMO is pinned to the Fermi-level, which is characteristic of systems exhibiting charge transfer.[54–56] To investigate this, we computed the ionization energies for **2A** and **2B** to be 4.0 eV, which is considerably lower than the computed Au(111) work function of 5.1 eV (Figure S6a). Additionally, we performed Bader's atoms in molecules (AIM) analysis[57,58] on the DFT charge density of the adsorbed systems, and obtained a charge transfer of 1.25 and 1.17 electrons from the molecules to the metal surface for **2A** and **2B**, respectively. Charge density redistribution calculations (Figure S6b,c) clearly reflect this charge transfer, and in addition reveal some intramolecular charge redistribution due to weak hybridization with substrate orbitals that is most pronounced on the p$_z$ orbitals of the edge carbons which are closest to the substrate.
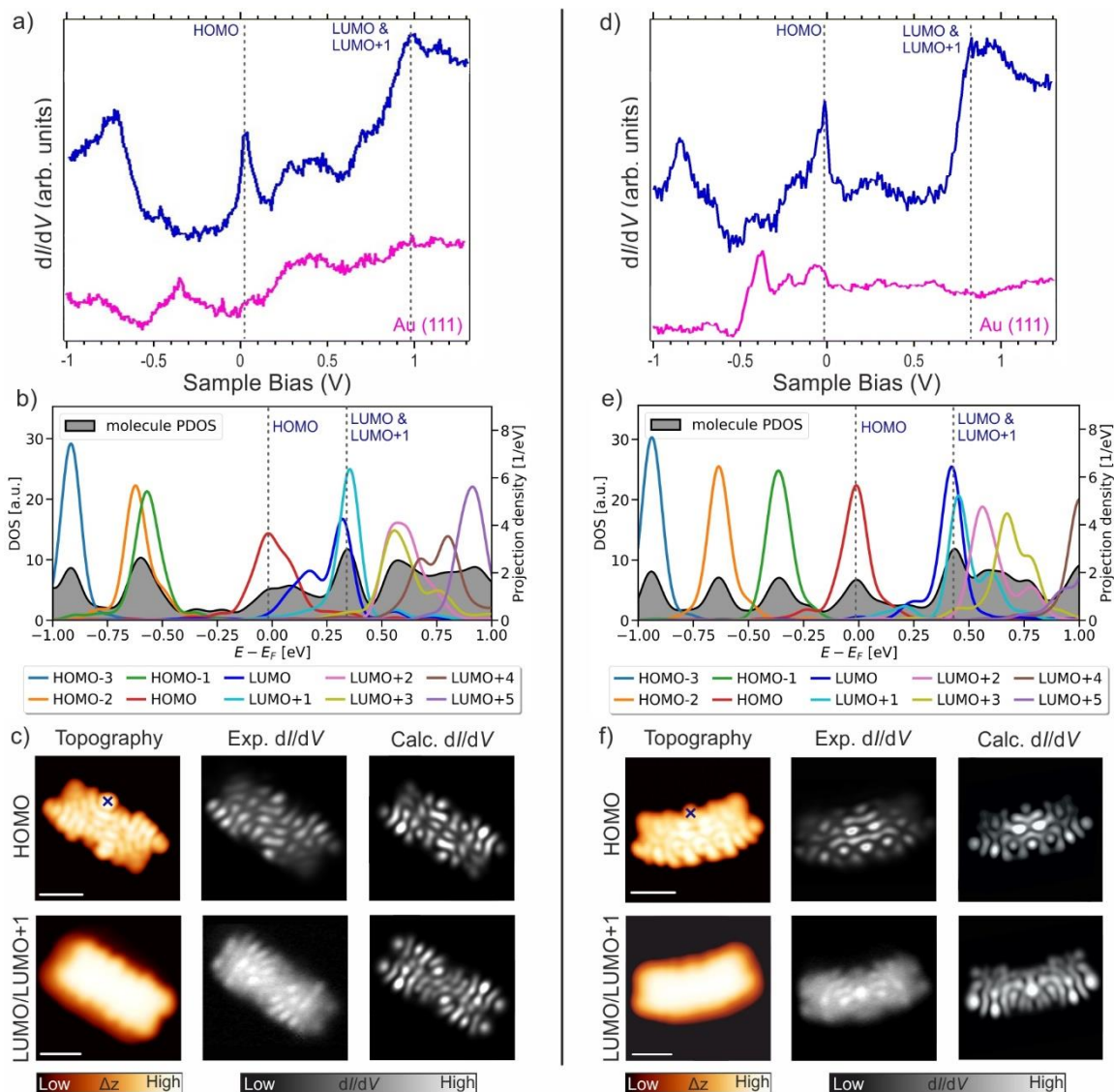
**Figure 3. Electronic properties of 2A and 2B on Au(111).** a,d) d$I$/d$V$ spectra of **2A** and **2B**, respectively, acquired on the nanographenes at the positions indicated by the blue cross, and reference spectra taken on the bare Au(111) surface (pink lines). b,e) Projected density of states (PDOS; left y-axis) on the molecule for the DFT-optimized NGs on Au(111), and projection of the orbitals of the gas-phase NGs to the orbitals of the NG/Au(111) (right y-axis). Gaussian broadening applied with FWHM of 0.1 eV. c,f) High-resolution STM images (left), simultaneously acquired constant-height differential conductance (d$I$/d$V$) maps (center) and corresponding DFT-calculated LDOS maps (right) at the energetic positions corresponding to the HOMO (top) and the LUMO/LUMO+1 peak (bottom) of **2A** and **2B**, respectively. Tunneling parameters for the STM images and the associated d$I$/d$V$ maps: c) HOMO ($V_b$ = 17 mV, $I_t$ = 100 pA); LUMO/LUMO+1 ($V_b$ = 800 mV, $I_t$ = 150 pA), f) HOMO ($V_b$ = -20 mV, $I_t$ = 100 pA); LUMO/LUMO+1 ($V_b$ = 750 mV V, $I_t$ = 100 pA). All scale bars: 1 nm.

To characterize the magnetic ground states of **2A** and **2B** in the gas phase, we performed restricted and unrestricted DFT calculations at the B3LYP/6-311+G** level of theory. In both cases, the ground state turned out to be the open-shell singlet with moderate biradical character of y=0.61 and y=0.33 for **2A** and **2B**, respectively (Table S1). The resulting spin densities shown in Figure 4a,b indicate that the maximum spin densities are located at the outer edges of two heptagonal rings. Additionally, we characterized the local aromaticity pattern of the molecules with the NICS$_{zz}$(1) GIAO-B3LYP method (Figure 4c,d), showing large overall aromaticity with average NICS values of -6.7 ppm and -5.9 ppm for **2A** and **2B**, respectively. The (hypothetical) NGs without ring rearrangements, that is, **2A-e** and **2B-e**, show considerably higher biradical character of y=0.78 and 0.86, respectively, (Table S1) and anti-aromaticity (Figure S2), which further manifest their lower stability compared to the observed products **2A** and **2B**.
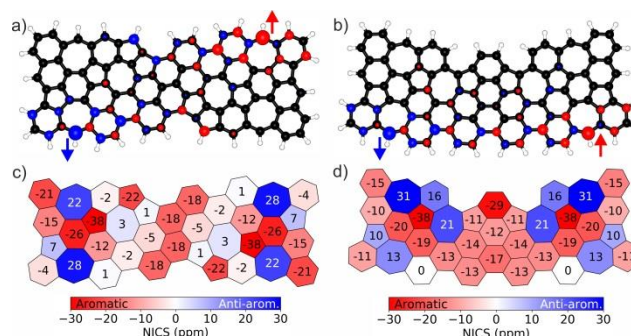


**Figure 4. Computational characterization of the electronic structure of 2A and 2B.** a,b) Spin densities of the open-shell singlet ground state of **2A** and **2B** at the UB3LYP level of theory. Isovalues at +-0.005 a.u. are shown. The highest amplitude of spin density indicates the locations of radical sites (arrows). c,d) Local aromaticity patterns of **2A** and **2B** calculated with the

NICS$_{zz}$(1) GIAO-B3LYP method. For comparison, at the same level of theory, benzene NICS$_{zz}$(1) value is -29.3 ppm and biphenylene's anti-aromatic 4-carbon ring NICS$_{zz}$(1) value is 37.2 ppm.

In conclusion, we have demonstrated the sequential on-surface synthesis of well-defined NGs **2A** and **2B** containing odd-membered polycycles on Au(111) from precursor **1**. The expected dehalogenation and oxidative ring-closure reactions of the four methyl substituents afford the formation of four heptagonal rings per nanographene upon annealing at 300°C. Further thermal activation at 340°C induces a ring rearrangement reaction driven by intramolecular structural strain where two additional heptagonal rings and pentalene and *as*-indacene segments are formed for **2A** and **2B**, respectively. The chemical structures of **2A** and **2B** have been elucidated by STM and nc-AFM. STS studies reveal that **2A** and **2B** exhibit narrow experimental frontier electronic gaps of 0.96 and 0.85 eV on Au(111), respectively, with moderate open-shell characters in gas phase elucidated by ab initio calculations, and a considerable charge transfer from the NGs to the Au(111) surface upon adsorption. Our results motivate the rational fabrication of larger non-benzenoid ring topologies as functional centers toward the perspective of engineering graphene-based devices.

## ASSOCIATED CONTENT

**Supporting Information**. The Supporting Information is available free of charge on the ACS Publications website at DOI: . Experimental details, synthesis, characterizations, computational studies, and NMR spectra (PDF)

## AUTHOR INFORMATION

### Corresponding Author

*xinliang.feng@tu-dresden.de

*juliu@hku.hk

*roman.fasel@empa.ch

*jose-ignacio.urgel@empa.ch

### Present Addresses

$^{\phi}$IMDEA Nanoscience, C/ Faraday 9, Campus de Cantoblanco, 28049 Madrid, Spain

### Author Contributions

¶T.G.L., J.U. and K.E. contributed equally to this work.

### Notes
The authors declare no competing financial interest.

## REFERENCES

(1)      Novoselov, K. S. Electric Field Effect in Atomically Thin Carbon Films. *Science* **2004**, *306* (5696), 666–669.

(2)      Gao, Y.; Hao, P. Mechanical Properties of Monolayer Graphene under Tensile and Compressive Loading. *Phys. E Low-Dimens. Syst. Nanostructures* **2009**, *41* (8), 1561–1566.

(3)      Wang, Y.; Huang, Y.; Song, Y.; Zhang, X.; Ma, Y.; Liang, J.; Chen, Y. Room-Temperature Ferromagnetism of Graphene. *Nano Lett.* **2009**, *9* (1), 220–224.

(4)      Falkovsky, L. A. Optical Properties of Graphene. *J. Phys. Conf. Ser.* **2008**, *129*, 012004.

(5)      Castro Neto, A. H.; Guinea, F.; Peres, N. M. R.; Novoselov, K. S.; Geim, A. K. The Electronic Properties of Graphene. *Rev. Mod. Phys.* **2009**, *81* (1), 109–162.

(6)      Bae, S.; Kim, H.; Lee, Y.; Xu, X.; Park, J.-S.; Zheng, Y.; Balakrishnan, J.; Lei, T.; Ri Kim, H.; Song, Y. I.; Kim, Y.-J.; Kim, K. S.; Özyilmaz, B.; Ahn, J.-H.; Hong, B. H.; Iijima, S. Roll-to-Roll Production of 30-Inch Graphene Films for Transparent Electrodes. *Nat. Nanotechnol.* **2010**, *5* (8), 574–578.

(7)      Kim, K. S.; Zhao, Y.; Jang, H.; Lee, S. Y.; Kim, J. M.; Kim, K. S.; Ahn, J.-H.; Kim, P.; Choi, J.-Y.; Hong, B. H. Large-Scale Pattern Growth of Graphene Films for Stretchable Transparent Electrodes. *Nature* **2009**, *457* (7230), 706–710.

(8)      Eda, G.; Fanchini, G.; Chhowalla, M. Large-Area Ultrathin Films of Reduced Graphene Oxide as a Transparent and Flexible Electronic Material. *Nat. Nanotechnol.* **2008**, *3* (5), 270–274.

(9)      Jornet, J. M.; Akyildiz, I. F. Graphene-Based Nano-Antennas for Electromagnetic Nanocommunications in the Terahertz Band. In *Proceedings of the Fourth European Conference on Antennas and Propagation*; 2010; pp 1–5.

(10)      Schedin, F.; Geim, A. K.; Morozov, S. V.; Hill, E. W.; Blake, P.; Katsnelson, M. I.; Novoselov, K. S. Detection of Individual Gas Molecules Adsorbed on Graphene. *Nat. Mater.* **2007**, *6* (9), 652–655.

(11)      Bunch, J. S.; Zande, A. M. van der; Verbridge, S. S.; Frank, I. W.; Tanenbaum, D. M.; Parpia, J. M.; Craighead, H. G.; McEuen, P. L. Electromechanical Resonators from Graphene Sheets. *Science* **2007**, *315* (5811), 490–493.

(12)      Novoselov, K. S.; Geim, A. K.; Morozov, S. V.; Jiang, D.; Katsnelson, M. I.; Grigorieva, I. V.; Dubonos, S.

V.; Firsov, A. A. Two-Dimensional Gas of Massless Dirac Fermions in Graphene. *Nature* **2005**, *438* (7065), 197–200.

(13) Talirz, L.; Ruffieux, P.; Fasel, R. On-Surface Synthesis of Atomically Precise Graphene Nanoribbons. *Adv. Mater.* **2016**, *28* (29), 6222–6231.

(14) Fujii, S.; Enoki, T. Nanographene and Graphene Edges: Electronic Structure and Nanofabrication. *Acc. Chem. Res.* **2013**, *46* (10), 2202–2210.

(15) Banhart, F.; Kotakoski, J.; Krasheninnikov, A. V. Structural Defects in Graphene. *ACS Nano* **2011**, *5* (1), 26–41.

(16) Araujo, P. T.; Terrones, M.; Dresselhaus, M. S. Defects and Impurities in Graphene-like Materials. *Mater. Today* **2012**, *15* (3), 98–109.

(17) Chen, L.; Hernandez, Y.; Feng, X.; Müllen, K. From Nanographene and Graphene Nanoribbons to Graphene Sheets: Chemical Synthesis. *Angew. Chem. Int. Ed.* **2012**, *51* (31), 7640–7654.

(18) Wu, J.; Pisula, W.; Müllen, K. Graphenes as Potential Material for Electronics. *Chem. Rev.* **2007**, *107* (3), 718–747.

(19) Narita, A.; Wang, X.-Y.; Feng, X.; Müllen, K. New Advances in Nanographene Chemistry. *Chem. Soc. Rev.* **2015**, *44* (18), 6616–6643.

(20) Chong, Y.; Ma, Y.; Shen, H.; Tu, X.; Zhou, X.; Xu, J.; Dai, J.; Fan, S.; Zhang, Z. The in Vitro and in Vivo Toxicity of Graphene Quantum Dots. *Biomaterials* **2014**, *35* (19), 5041–5048.

(21) Sun, Z.; Wu, J. Open-Shell Polycyclic Aromatic Hydrocarbons. *J. Mater. Chem.* **2012**, *22* (10), 4151–4160.

(22) Liu, C.; Sandoval-Salinas, M. E.; Hong, Y.; Gopalakrishna, T. Y.; Phan, H.; Aratani, N.; Herng, T. S.; Ding, J.; Yamada, H.; Kim, D.; Casanova, D.; Wu, J. Macrocyclic Polyradicaloids with Unusual Super-Ring Structure and Global Aromaticity. *Chem* **2018**, *4* (7), 1586–1595.

(23) Yamamoto, K.; Ie, Y.; Tohnai, N.; Kakiuchi, F.; Aso, Y. Antiaromatic Character of Cycloheptatriene-Bis-Annelated Indenofluorene Framework Mainly Originated from Heptafulvene Segment. *Sci. Rep.* **2018**, *8* (1), 17663.

(24) Mishra, S.; Lohr, T. G.; Pignedoli, C. A.; Liu, J.; Berger, R.; Urgel, J. I.; Müllen, K.; Feng, X.; Ruffieux, P.; Fasel, R. Tailoring Bond Topologies in Open-Shell Graphene Nanostructures. *ACS Nano* **2018**, *12* (12), 11917–11927.

(25) Di Giovannantonio, M.; Eimre, K.; Yakutovich, A. V.; Chen, Q.; Mishra, S.; Urgel, J. I.; Pignedoli, C. A.; Ruffieux, P.; Müllen, K.; Narita, A.; Fasel, R. On-Surface Synthesis of Antiaromatic and Open-Shell Indeno[2,1-b]Fluorene Polymers and Their Lateral Fusion into Porous Ribbons. *J. Am. Chem. Soc.* **2019**, *141* (31), 12346–12354.

(26) Müllen, K.; Rabe, J. P. Nanographenes as Active Components of Single-Molecule Electronics and How a Scanning Tunneling Microscope Puts Them To Work. *Acc. Chem. Res.* **2008**, *41* (4), 511–520.

(27) Urgel, J. I.; Di Giovannantonio, M.; Segawa, Y.; Ruffieux, P.; Scott, L. T.; Pignedoli, C. A.; Itami, K.; Fasel, R. Negatively Curved Warped Nanographene Self-Assembled on Metal Surfaces. *J. Am. Chem. Soc.* **2019**, *141* (33), 13158–13164.

(28) Liu, J.; Mishra, S.; Pignedoli, C. A.; Passerone, D.; Urgel, J. I.; Fabrizio, A.; Lohr, T. G.; Ma, J.; Komber, H.; Baumgarten, M.; Corminboeuf, C.; Berger, R.; Ruffieux, P.; Müllen, K.; Fasel, R.; Feng, X. Open-Shell Nonbenzenoid Nanographenes Containing Two Pairs of Pentagonal and Heptagonal Rings. *J. Am. Chem. Soc.* **2019**, *141* (30), 12011–12020.

(29) Xu, K.; Urgel, J. I.; Eimre, K.; Di Giovannantonio, M.; Keerthi, A.; Komber, H.; Wang, S.; Narita, A.; Berger, R.; Ruffieux, P.; Pignedoli, C. A.; Liu, J.; Müllen, K.; Fasel, R.; Feng, X. On-Surface Synthesis of a Nonplanar Porous Nanographene. *J. Am. Chem. Soc.* **2019**, *141* (19), 7726–7730.

(30) Rogers, C.; Chen, C.; Pedramrazi, Z.; Omrani, A. A.; Tsai, H.-Z.; Jung, H. S.; Lin, S.; Crommie, M. F.; Fischer, F. R. Closing the Nanographene Gap: Surface-Assisted Synthesis of Peripentacene from 6,6′-Bipentacene Precursors. *Angew. Chem. Int. Ed.* **2015**, *54* (50), 15143–15146.

(31) Fan, Q.; Martin-Jimenez, D.; Werner, S.; Ebeling, D.; Koehler, T.; Vollgraff, T.; Sundermeyer, J.; Hieringer, W.; Schirmeisen, A.; Gottfried, J. M. On-Surface Synthesis and Characterization of a Cycloarene: C108 Graphene Ring. *J. Am. Chem. Soc.* **2019**.

(32) Hieulle, J.; Carbonell-Sanromà, E.; Vilas-Varela, M.; Garcia-Lekue, A.; Guitián, E.; Peña, D.; Pascual, J. I. On-Surface Route for Producing Planar Nanographenes with Azulene Moieties. *Nano Lett.* **2018**, *18* (1), 418–423.

(33) Zuzak, R.; Pozo, I.; Engelund, M.; Garcia-Lekue, A.; Vilas-Varela, M.; Alonso, J. M.; Szymonski, M.; Guitián, E.; Pérez, D.; Godlewski, S.; Peña, D. Synthesis and Reactivity of a Trigonal Porous Nanographene on a Gold Surface. *Chem. Sci.* **2019**, *10* (43), 10143–10148.

(34) Vilas-Varela, M.; Fatayer, S.; Majzik, Z.; Pérez, D.; Guitián, E.; Gross, L.; Peña, D. [19]Dendriphene: A 19-Ring Dendritic Nanographene. *Chem. – Eur. J.* **2018**, *24* (67), 17697–17700.

(35)    Treier, M.; Pignedoli, C. A.; Laino, T.; Rieger, R.; Müllen, K.; Passerone, D.; Fasel, R. Surface-Assisted Cyclodehydrogenation Provides a Synthetic Route towards Easily Processable and Chemically Tailored Nanographenes. *Nat. Chem.* **2011**, *3* (1), 61–67.

(36)    Wang, X.-Y.; Richter, M.; He, Y.; Björk, J.; Riss, A.; Rajesh, R.; Garnica, M.; Hennersdorf, F.; Weigand, J. J.; Narita, A.; Berger, R.; Feng, X.; Auwärter, W.; Barth, J. V.; Palma, C.-A.; Müllen, K. Exploration of Pyrazine-Embedded Antiaromatic Polycyclic Hydrocarbons Generated by Solution and on-Surface Azomethine Ylide Homocoupling. *Nat. Commun.* **2017**, *8* (1).

(37)    Wang, X.-Y.; Narita, A.; Müllen, K. Precision Synthesis versus Bulk-Scale Fabrication of Graphenes. *Nat. Rev. Chem.* **2017**, *2* (1), 1–10.

(38)    Shen, Q.; Gao, H.-Y.; Fuchs, H. Frontiers of On-Surface Synthesis: From Principles to Applications. *Nano Today* **2017**, *13*, 77–96.

(39)    Giovannantonio, M. D.; Contini, G. Reversibility and Intermediate Steps as Key Tools for the Growth of Extended Ordered Polymers via On-Surface Synthesis. *J. Phys. Condens. Matter* **2018**, *30* (9), 093001.

(40)    Moulay, S. THE MOST WELL-KNOWN REARRANGEMENTS IN ORGANIC CHEMISTRY AT HAND. *Chem. Educ. Res. Pract.* **2002**, *3* (1), 33–64.

(41)    de Oteyza, D. G.; Gorman, P.; Chen, Y.-C.; Wickenburg, S.; Riss, A.; Mowbray, D. J.; Etkin, G.; Pedramrazi, Z.; Tsai, H.-Z.; Rubio, A.; Crommie, M. F.; Fischer, F. R. Direct Imaging of Covalent Bond Structure in Single-Molecule Chemical Reactions. *Science* **2013**, *340* (6139), 1434–1437.

(42)    Riss, A.; Paz, A. P.; Wickenburg, S.; Tsai, H.-Z.; De Oteyza, D. G.; Bradley, A. J.; Ugeda, M. M.; Gorman, P.; Jung, H. S.; Crommie, M. F.; Rubio, A.; Fischer, F. R. Imaging Single-Molecule Reaction Intermediates Stabilized by Surface Dissipation and Entropy. *Nat. Chem.* **2016**, *8* (7), 678–683.

(43)    Shiotari, A.; Nakae, T.; Iwata, K.; Mori, S.; Okujima, T.; Uno, H.; Sakaguchi, H.; Sugimoto, Y. Strain-Induced Skeletal Rearrangement of a Polycyclic Aromatic Hydrocarbon on a Copper Surface. *Nat. Commun.* **2017**, *8* (1), 16089.

(44)    Li, J.; Sanz, S.; Corso, M.; Choi, D. J.; Peña, D.; Frederiksen, T.; Pascual, J. I. Single Spin Localization and Manipulation in Graphene Open-Shell Nanostructures. *Nat. Commun.* **2019**, *10* (1), 1–7.

(45)    Pavliček, N.; Gawel, P.; Kohn, D. R.; Majzik, Z.; Xiong, Y.; Meyer, G.; Anderson, H. L.; Gross, L. Polyyne Formation via Skeletal Rearrangement Induced by Atomic Manipulation. *Nat. Chem.* **2018**, *10* (8), 853–858.

(46)    Sun, Q.; Zhang, C.; Li, Z.; Kong, H.; Tan, Q.; Hu, A.; Xu, W. On-Surface Formation of One-Dimensional Polyphenylene through Bergman Cyclization. *J. Am. Chem. Soc.* **2013**, *135* (23), 8448–8451.

(47)    Schuler, B.; Fatayer, S.; Mohn, F.; Moll, N.; Pavliček, N.; Meyer, G.; Peña, D.; Gross, L. Reversible Bergman Cyclization by Atomic Manipulation. *Nat. Chem.* **2016**, *8* (3), 220–224.

(48)    Gross, L.; Mohn, F.; Moll, N.; Liljeroth, P.; Meyer, G. The Chemical Structure of a Molecule Resolved by Atomic Force Microscopy. *Science* **2009**, *325* (5944), 1110–1114.

(49)    Weiss, C.; Wagner, C.; Temirov, R.; Tautz, F. S. Direct Imaging of Intermolecular Bonds in Scanning Tunneling Microscopy. *J. Am. Chem. Soc.* **2010**, *132* (34), 11864–11865.

(50)    Gross, L. Recent Advances in Submolecular Resolution with Scanning Probe Microscopy. *Nat. Chem.* **2011**, *3* (4), 273–278.

(51)    Pavliček, N.; Mistry, A.; Majzik, Z.; Moll, N.; Meyer, G.; Fox, D. J.; Gross, L. Synthesis and Characterization of Triangulene. *Nat. Nanotechnol.* **2017**, *12* (4), 308–311.

(52)    Urgel, J. I.; Mishra, S.; Hayashi, H.; Wilhelm, J.; Pignedoli, C. A.; Giovannantonio, M. D.; Widmer, R.; Yamashita, M.; Hieda, N.; Ruffieux, P.; Yamada, H.; Fasel, R. On-Surface Light-Induced Generation of Higher Acenes and Elucidation of Their Open-Shell Character. *Nat. Commun.* **2019**, *10* (1), 861.

(53)    Zuzak, R.; Dorel, R.; Krawiec, M.; Such, B.; Kolmer, M.; Szymonski, M.; Echavarren, A. M.; Godlewski, S. Nonacene Generated by On-Surface Dehydrogenation. *ACS Nano* **2017**, *11* (9), 9321–9329.

(54)    Braun, S.; Salaneck, W. R.; Fahlman, M. Energy-Level Alignment at Organic/Metal and Organic/Organic Interfaces. *Adv. Mater.* **2009**, *21* (14–15), 1450–1472.

(55)    Merino-Díez, N.; Garcia-Lekue, A.; Carbonell-Sanromà, E.; Li, J.; Corso, M.; Colazzo, L.; Sedona, F.; Sánchez-Portal, D.; Pascual, J. I.; de Oteyza, D. G. Width-Dependent Band Gap in Armchair Graphene Nanoribbons Reveals Fermi Level Pinning on Au(111). *ACS Nano* **2017**, *11* (11), 11661–11668.

(56)    Faraggi, M. N.; Jiang, N.; Gonzalez-Lakunza, N.; Langner, A.; Stepanow, S.; Kern, K.; Arnau, A. Bonding and Charge Transfer in Metal–Organic Coordination Networks on Au(111) with Strong Acceptor Molecules. *J. Phys. Chem. C* **2012**, *116* (46), 24558–24565.

(57)    Orville-Thomas, W. J. Atoms in Molecules — a Quantum Theory: Richard F.W. Bader, Clarendon Press,

Oxford, U.K. 1994, 438 Pp., £25. *J. Mol. Struct. THEOCHEM* **1996**, *360* (1), 175.

(58)  Tang, W.; Sanville, E.; Henkelman, G. A Grid-Based Bader Analysis Algorithm without Lattice Bias. *J. Phys. Condens. Matter* **2009**, *21* (8), 084204.

Insert Table of Contents artwork here